Monitoring the Optical/UV Transmission of the HRC with Betelgeuse

J. Posson-Brown, V. Kashyap (CXC/SAO)

31 Oct 2005

Abstract

We have carried out a comprehensive analysis of all Betelgeuse calibration observations obtained to date with the HRC. Betelgeuse is undetected in all of the individual observations as well as cumulatively. We find that the expected exposure time for detection is > 1 Ms for aimpoint observations for both HRC-I and HRC-S. We also find that the predicted count rate due to the UV/optical flux is sufficient to have already resulted in a detection for observations carried out over the thin filter regions at large off-axis angles of the HRC-S. The non-detections therefore suggest that the out-of-band response must be decreased, by a factor < 0.3.

Name	**Class**	m_V	$B-V$	**Distance**
α Ori	M1 Iab	0.58	1.77	131 pc

`Stellar paramenters for Betelgeuse.`

Data

Date	ObsId	Exposure Time (s)
7 Dec 2001	2595	1892.10
6 Feb 2003	3680	1893.38
2 Feb 2004	5055	2075.88
2 Feb 2005	5970	2129.42

Table 1: HRC-I observations of Betelgeuse. The listed exposure times are corrected for deadtime. Note that deadtime is not a concern for these observations, as the maximum count rate is < 146 ct s^{-1} (typically around 30 ct s^{-1}), which is safely under the telemetry saturation limit of 184 ct s^{-1}. All observations are carried out close to the nominal aimpoint, at $(Y, Z) = (0', 0')$.

Data, continued

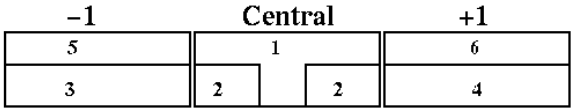

Figure 1: Sketch showing the arrangement of UVIS-S segments. Segments marked 1, 5, and 6 have larger thicknesses of polyimide and Al than segments marked 2, 3, and 4. The spacecraft Y-axis is aligned along the long axis and increases from right to left, while the Z-axis is aligned along the short axis and increases from bottom to top.

Date	ObsId	Exposure Time (s)	(Y, Z) Offset (′)
7 Dec 2001	2596	1926.67	0, 0
7 Dec 2001	2597	2167.22	-10, 0
7 Dec 2001	2598	1997.21	-20, 0
7 Dec 2001	2599	1297.95	-20, -3
6 Feb 2003	3681	1819.59	0, 0
6 Feb 2003	3682	2131.18	-10, 0
6 Feb 2003	3683	1903.91	-20, 0
6 Feb 2003	3684	2002.92	-20, -3
2 Feb 2004	5056	1945.28	0, 0
2 Feb 2004	5057	1467.02	-10, 0
2 Feb 2004	5058	1555.90	-20, 0
2 Feb 2004	5059	464.20	-20, -3
2 Feb 2005	5971	2140.42	0, 0
2 Feb 2005	5972	2148.69	-10, 0
2 Feb 2005	5973	998.37	-20, 0
2 Feb 2005	5974	1601.16	-20, -3

Table 2: HRC-S observations of Betelgeuse. Y offsets are along the dispersion axis and Z offsets are across the dispersion axis. As with the HRC-I data (Table 1), deadtime corrections are a minor factor, with the maximum count rate being < 170 ct s^{-1} (typically 40 ct s^{-1} for the wing plate and less than that for the central plate).

Analysis

- Used standard level 2 processing, plus additional time-filtering for off-axis HRC-S observations to remove times affected by strong background flaring
- Measured background-subtracted count rate at location of source (square points in Figures 4-7)
- Computed 99.7% confidence count rate upper limits (triangular points in Figures 4-7)
- Computed expected count rates (red dashed lines in Figures 4-7) by folding spectral model of Betelgeuse (shown in Figure 2) with appropriate model of the detector response to out-of-band radiation derived from pre-flight calibration measurements (see Figure 3)

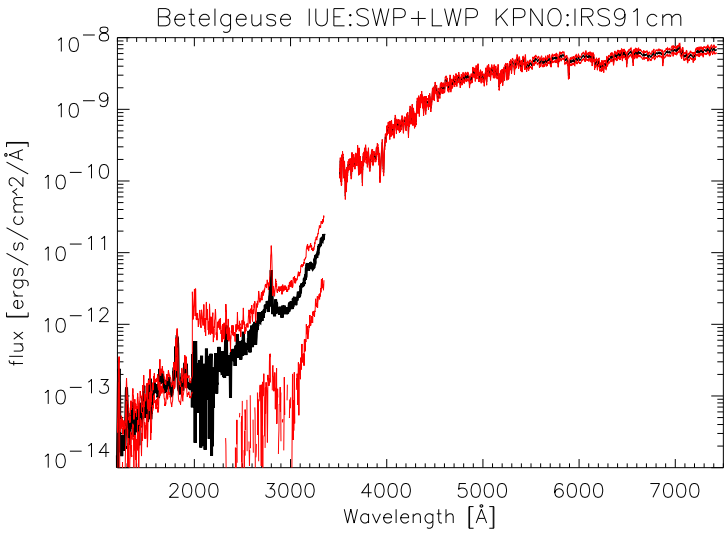

Figure 2: UV/optical spectral model for Betelgeuse. The UV part is derived from averaging its IUE spectra, and the optical part by normalizing standards spectra to its optical flux. The break at 3500Å is connected by linear interpolation. The statistical 1σ error band is shown in red.

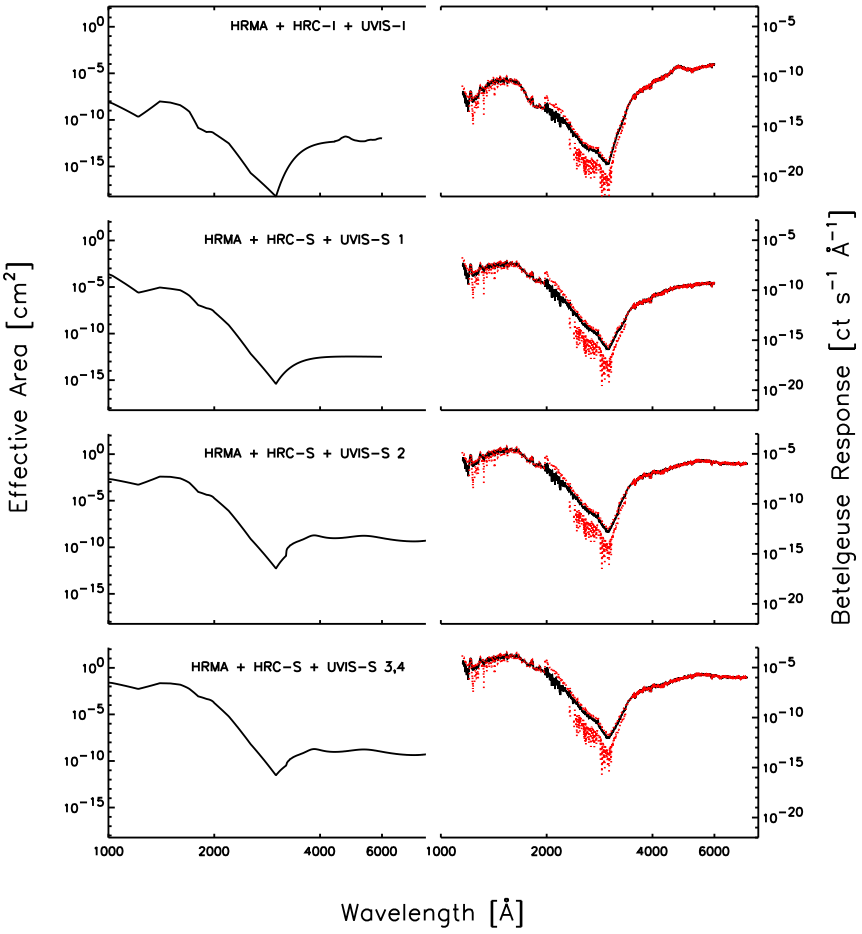

Figure 3: The HRC out-of-band effective area and the response to Betelgeuse. Each row of plots refers, sequentially, to data acquired under the filters (see Figure 1) UVIS-I, UVIS-S1, UVIS-S2, and UVIS-S3. (Note that UVIS-S3 is identical to UVIS-S4.) The figures to the left show the effective area; those to the right depict the predicted response of the detector to Betelgeuse. Note that despite the small intrinsic UV flux of Betelgeuse (Figure 2), the predicted count rate due to the UV leak is generally greater than to the red leak.

The next four figures (4-7) show background-subtracted estimates of the net source rates (squares) along with their estimated errors (solid vertical lines). The expected count rates due to the UV/optical flux from Betelgeuse are also shown as red dashed lines, with the error, if nontrivial, shown as red dotted lines. In all cases, the net count rates are consistent with there having been no detection. Upper limits computed at a 99.7% significance level are also shown (inverted triangles).

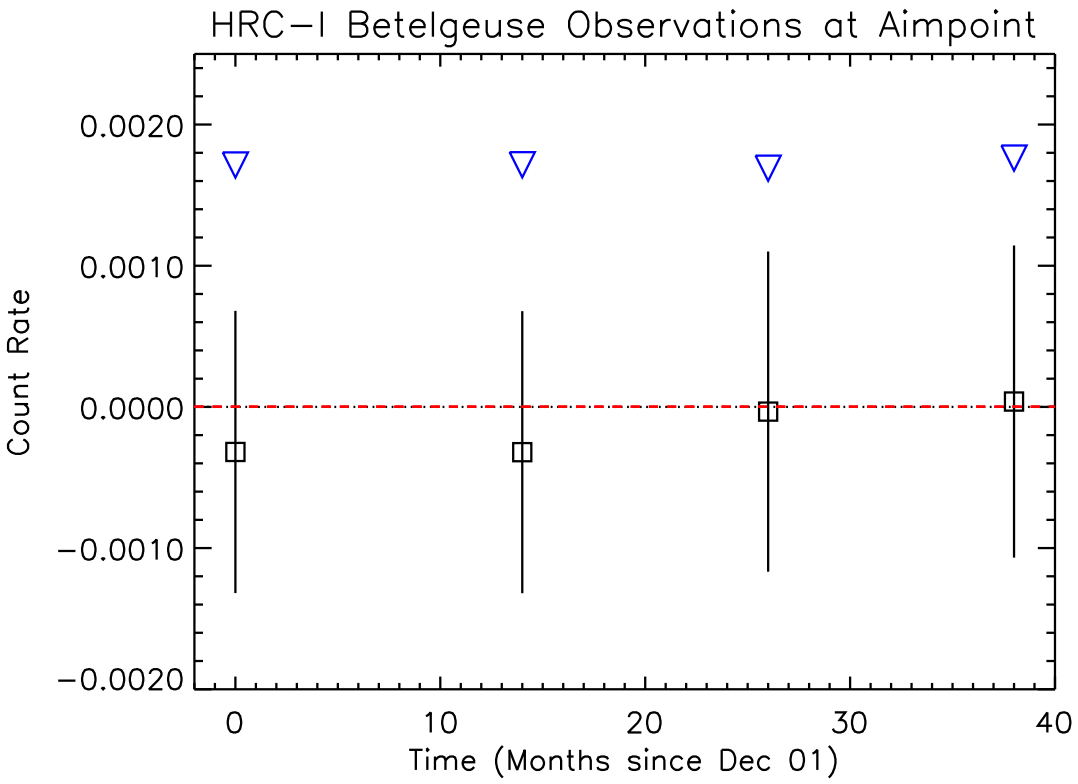

Figure 4: HRC-I+UVIS-I

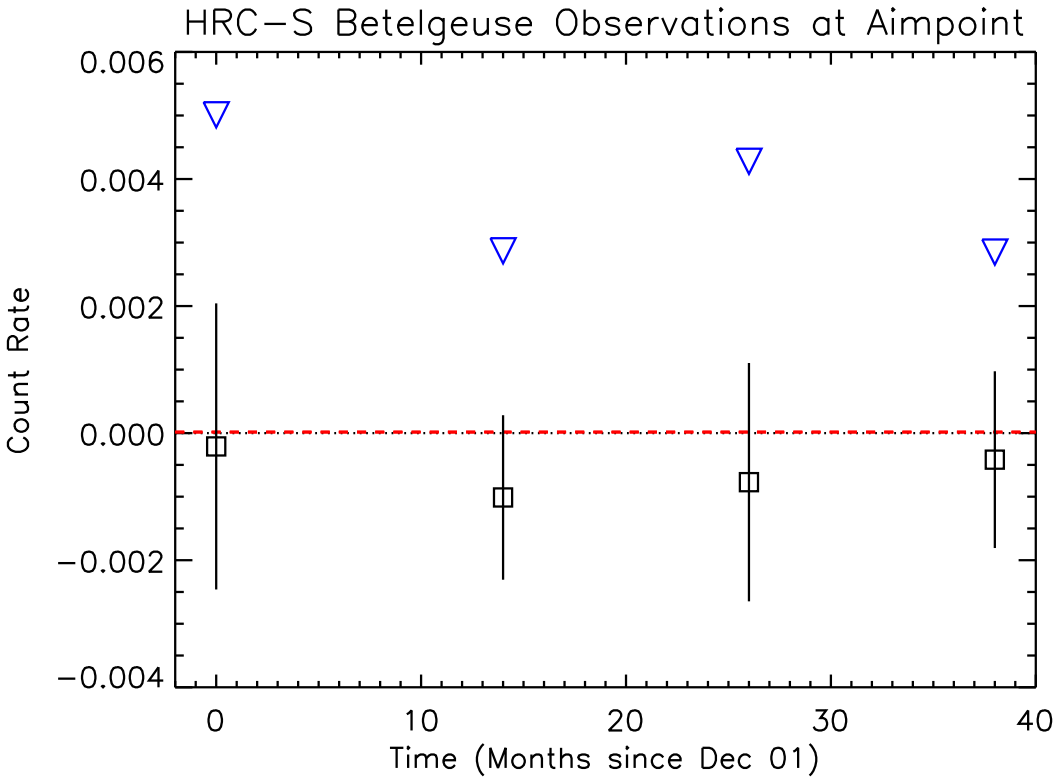

Figure 5: HRC-S at the aimpoint, sampling segment 1 of the UVIS-S

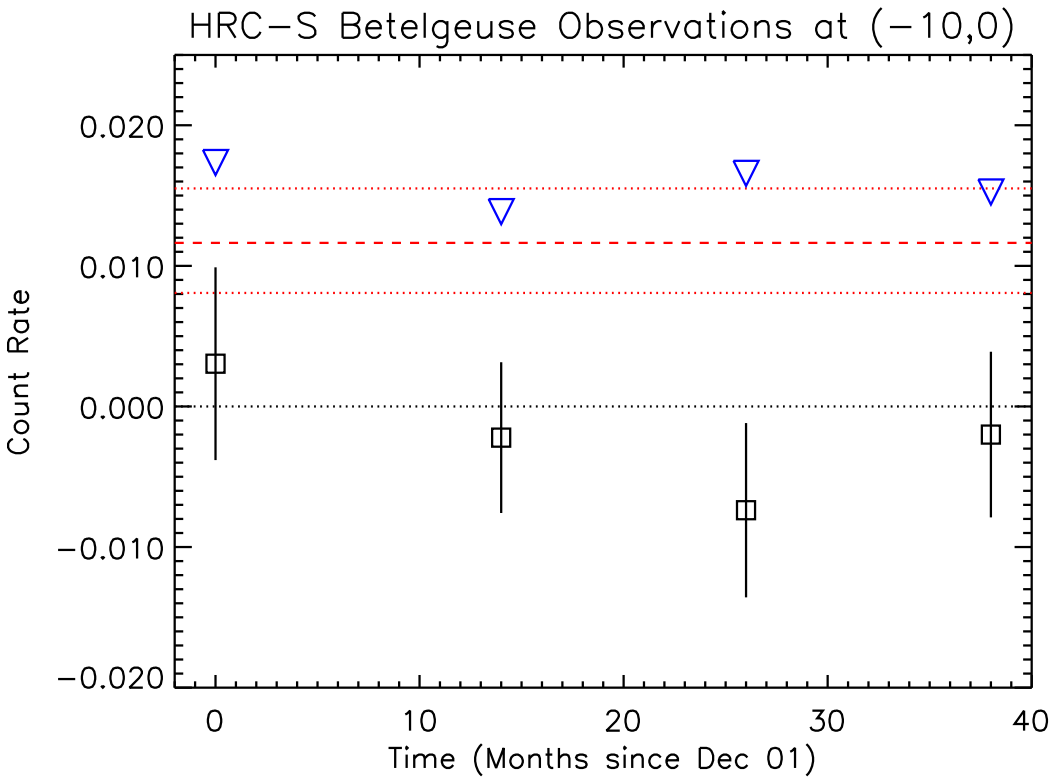

Figure 6: HRC-S at the offset pointing of $(Y,Z) = (-10', 0')$, sampling segment 2 of the UVIS-S

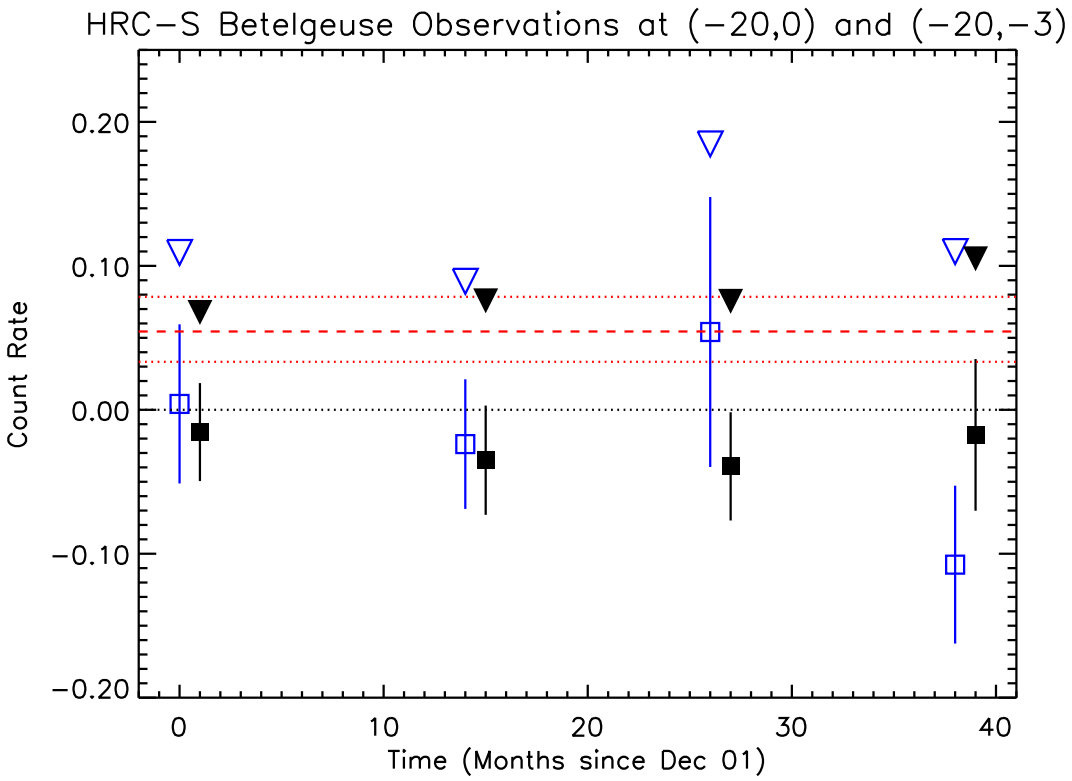

Figure 7:HRC-S data at $(Y,Z) = (-20', 0')$ and $(Y,Z) = (-20', -3')$, sampling segment 3 of the UVIS-S. ($(Y,Z) = (-20', 0')$ are denoted with filled symbols, and $(Y,Z) = (-20', -3')$ with open symbols, offset for clarity

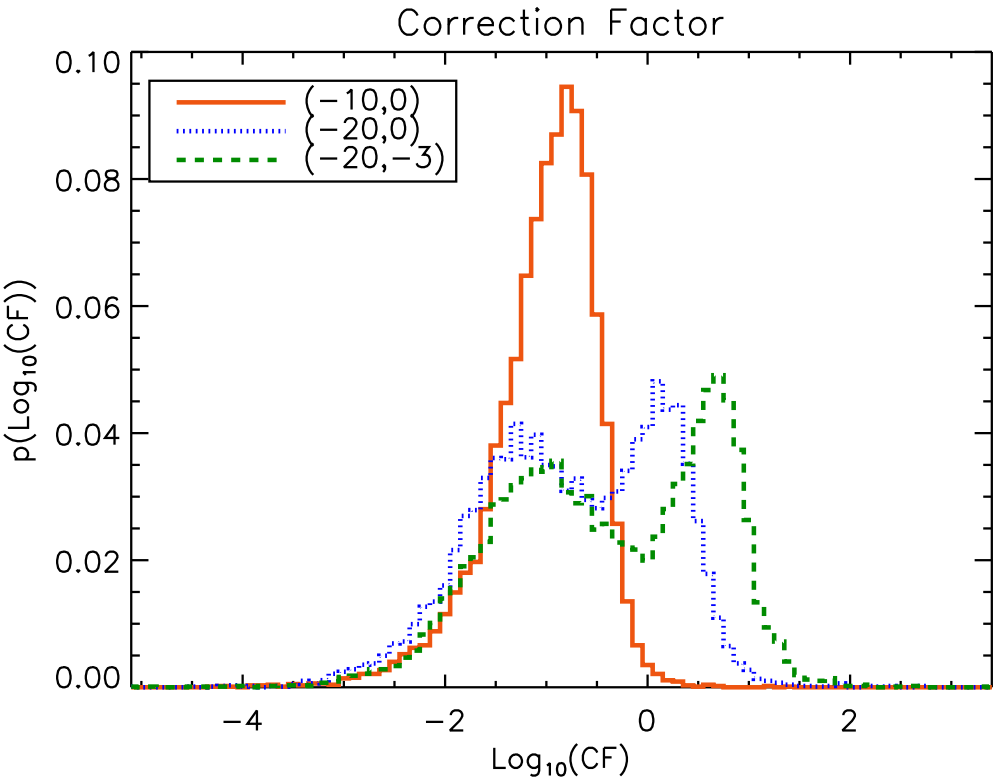

Figure 8: Probability distribution of the factor with which to correct the out-of-band HRC-S+UVIS-S response. The ratios of the observed to the predicted source intensities are generated during a Monte Carlo analysis that takes into account the errors in the measurements of the UV/optical flux, the counts in the background region, and the background-to-source scaling factors for the outer-wing data. The distributions for HRC-S+UVIS-S2 ($(Y,Z)=(-10',0')$ - solid curve), and HRC-S+UVIS-S3 ($(Y,Z)=(-20',0')$ - dotted curve; $(Y,Z)=(-20',-3')$ - dashed curve) are shown. The latter show a bimodal behavior that is due to the uncertainties inherent in the determination of a proper background rate at the locations of the source. The 68% confidence range on the correction factor, derived from the unimodal distribution of the correction factor for HRC-S+UVIS-S2, is $0.03-0.3$.

Filter	**Expected count rate** [ct s^{-1}]	**Accumulated Exposure** [s]	**Upper Limit** [ct s^{-1}]	**Required Exposure**
UVIS-I	$1.29^{+0.11}_{-0.14} \times 10^{-6}$	7991	7.04×10^{-4}	> 1 Ms
UVIS-S 1 (center, thick)	$1.64^{+0.86}_{-0.71} \times 10^{-5}$	7832	1.86×10^{-3}	> 1 Ms
UVIS-S 2 (center, thin)	$1.16^{+0.39}_{-0.36} \times 10^{-2}$	7914	7.86×10^{-3}	3.5 ks
UVIS-S 3,4 (outer, thin)	$5.44^{+2.36}_{-2.14} \times 10^{-2}$	11822	2.91×10^{-2}	3.4 ks

Table 4: Summary of the HRC observations of Betelgeuse. The predicted count rates (and 1σ bounds) based on the UV/optical flux of Betelgeuse are compared with the upper limits derived from the accumulated data, and the time required for a detection at 99.7% significance is noted.

References

– Jacoby, G.H., Hunter D.A., & Christian C.A., 1984, ApJS, 56, 257

– van Dyk, D., Connors, A., Kashyap, V.L., & Siemiginowska, A., 2001, ApJ, 548, 224

– Zombeck, M., 1999, *CXC Memo*, http://asc.harvard.edu/cal/Hrc/Documents/Zombeck/

– Zombeck, M.V., Barbera, M., Butt, Y., Drake, J.J., Harnden, F.R.,Jr., Murray, S.S., & Wargelin, B., 2000, *X-Ray Astronomy 2000, Palermo*, http://hea-www.harvard.edu/HRC/calib/palermopaper.ps